ORIGINAL RESEARCH

Sustained release of anticancer agent phytic acid from its chitosan-coated magnetic nanoparticles for drug-delivery system

Farahnaz Barahuie[1,2]
Dena Dorniani[1,3,*]
Bullo Saifullah[1,*]
Sivapragasam Gothai[4]
Mohd Zobir Hussein[1]
Ashok Kumar Pandurangan[5]
Palanisamy Arulselvan[4]
Mohd Esa Norhaizan[6]

[1]Materials Synthesis and Characterization Laboratory, Institute of Advanced Technology, Universiti Putra Malaysia, Serdang, Selangor, Malaysia; [2]Zabol University of Medical Sciences, Zabol, Iran; [3]Department of Chemistry, University of Sheffield, Sheffield, UK; [4]Laboratory of Vaccines and Immunotherapeutics, Institute of Bioscience, Universiti Putra Malaysia, Serdang, Selangor, Malaysia; [5]Department of Pharmacology, Faculty of Medicine, University of Malaya, Kuala Lumpur, Malaysia; [6]Department of Nutrition and Dietetics, Faculty of Medicine and Health Sciences, Universiti Putra Malaysia, Serdang, Selangor, Malaysia

*These authors contributed equally to this work

Correspondence: Mohd Esa Norhaizan
Department of Nutrition and Dietetics, Faculty of Medicine and Health Sciences, Universiti Putra Malaysia, 43400 Serdang, Selangor, Malaysia
Tel +60 3 8947 2427
Fax +60 3 8942 6769
Email nhaizan@upm.edu.my

Abstract: Chitosan (CS) iron oxide magnetic nanoparticles (MNPs) were coated with phytic acid (PTA) to form phytic acid-chitosan-iron oxide nanocomposite (PTA-CS-MNP). The obtained nanocomposite and nanocarrier were characterized by powder X-ray diffraction, Fourier transform infrared spectroscopy, vibrating sample magnetometry, transmission electron microscopy, and thermogravimetric and differential thermogravimetric analyses. Fourier transform infrared spectra and thermal analysis of MNPs and PTA-CS-MNP nanocomposite confirmed the binding of CS on the surface of MNPs and the loading of PTA in the PTA-CS-MNP nanocomposite. The coating process enhanced the thermal stability of the anticancer nanocomposite obtained. X-ray diffraction results showed that the MNPs and PTA-CS-MNP nanocomposite are pure magnetite. Drug loading was estimated using ultraviolet-visible spectroscopy and showing a 12.9% in the designed nanocomposite. Magnetization curves demonstrated that the synthesized MNPs and nanocomposite were superparamagnetic with saturation magnetizations of 53.25 emu/g and 42.15 emu/g, respectively. The release study showed that around 86% and 93% of PTA from PTA-CS-MNP nanocomposite could be released within 127 and 56 hours by a phosphate buffer solution at pH 7.4 and 4.8, respectively, in a sustained manner and governed by pseudo-second order kinetic model. The cytotoxicity of the compounds on HT-29 colon cancer cells was evaluated by 3-(4,5-dimethylthiazol-2-yl)-2,5-diphenyltetrazolium bromide assay. The HT-29 cell line was more sensitive against PTA-CS-MNP nanocomposite than PTA alone. No cytotoxic effect was observed on normal cells (3T3 fibroblast cells). This result indicates that PTA-CS-MNP nanocomposite can inhibit the proliferation of colon cancer cells without causing any harm to normal cell.

Keywords: nanocomposite, drug delivery, chitosan, phytic acid, HT-29 cell line, controlled release

Introduction

Nanotechnology has incredible potential for revolutionizing the medical world by developing personalized medicine both for diagnosis and therapy. Nanomedicine (nanosized therapeutics and imaging agents) has exhibited a strong growth in nanodrugs where designed ingenious biocompatible nanocomposites for drug delivery purposes. These nanocomposites are widely used as nanodelivery systems that enhance the biodistribution of drugs and selectively target diseased tissues while protecting healthy tissues.[1,2]

Various nanocarriers including liposomes,[3–6] cell-based nanocarriers,[7] polymers,[8] carbon materials,[9,10] dendrimers,[11] and inorganic nanoparticles[12,13] have been employed for gene and drug delivery systems, which have shown efficacy both in vitro and in vivo. Recently, much attention has been devoted to polymer-based nanoparticles (typically chitosan [CS]-iron

oxide nanoparticles) as novel cellular delivery vectors in cancer therapy because of their excellent properties such as high encapsulation efficiency, sustained release properties, effective and convenient routes of administration, less toxicity, endocytosis efficiency, surface modifying capacity, ability to differentiate between cancer and normal cells,[14] superparamagnetic behavior and contrast agent, and low health care cost.[15]

Iron oxide magnetic nanoparticles (MNPs) with general formula Fe_3O_4 have been widely used for delivery of various drugs owing to some advantages: ease of preparation, superparamagnetic property,[16–18] biocompatibility, external control, controllable parameters,[19,20] and hypothermal behavior.[21,22] However, these nanoparticles due to the presence of OH^- groups with a large surface area to volume ratio and dipole–dipole attraction without any surface coating will be agglomerated and the size of particles will increase. Therefore, it is necessary to use polymers in the coating process to prevent the nuclear growth of iron oxide, preclude nanoparticles aggregation, and reduce toxic effect.[23–25]

CS, a natural polymer and deacetylated derivative of chitin, is most commonly used as a coating material for nanoparticles in anticancer drug delivery systems because of its unique biological features including biocompatibility,[26] anti-carcinogenicity, biodegradability, nontoxicity, hydrophilicity,[23,27–29] and great antimicrobial property.[30] The CS polymer reacts with iron oxide nanoparticles through glycosidic bonds and improves the stability and chemical reactivity of nanoparticles.[31]

Extensive studies using CS-MNPs nanocarrier have been performed in recent years to enhance anticancer drug efficacy and reduce the side effects of the drug. For instance, Javid et al[32] demonstrated that CS-MNPs nanoreservoir with a higher drug loading capacity increased the drug efficiency and anticancer properties of doxorubicin. The results emphasized that doxorubicin-CS-MNP nanocomposite showed a greater growth inhibitory effect on ovarian cancer cells (A2780 and OVCAR-3) than free drug.[32]

Phytic acid (PTA; $C_6H_{18}O_{24}P_6$) is a natural compound discovered in 1903. It is the major storage form of phosphorous in plants and legumes, including wheat bran, corn, soy beans, rice bran, and nuts,[33] and it is reported to possess a broad range of pharmaceutical properties, such as antioxidant,[34,35] chemopreventive,[36,37] hepatoprotective, and anticancer properties. Many studies presented that PTA inhibited cancer cell growth in leukemia, prostate, breast, liver, colon, and skin cancers.[38–40] However, this anticancer drug has very short plasma half-life and is released very fast.

Therefore, considering the aforementioned advantages of CS-MNPs, we report here the synthesis of a new nanohybrid, phytic acid-chitosan-MNPs (PTA-CS-MNP). The objective of this research was to explore the potential use of CS-MNPs for the delivery of anticancer drug PTA. We investigated the sustained release behavior of PTA from CS-MNPs nanocarrier and evaluated the cytotoxic effects against cancer cells and normal fibroblast (3T3) cell lines in vitro.

Materials and methods
Materials
The chemicals in this study were of analytical grade and were used as received without further purification. PTA sodium salt from rice (molecular formula: $C_6H_{18}O_{24}P_6$ $xNa^+ \cdot yH_2O$; molecular weight: 660.04) with ≥90 purity and CS, deacetylated at 75%–85%, sodium amp salt (>98% purity; molecular weight: 371.4 g/mol) were acquired from Sigma-Aldrich (St Louis, MO, USA). Aqueous acetic acid solution (99.8%) was supplied by Hamburg Industries (Hamburg, Germany). Ferrous chloride tetrahydrate ($FeCl_2 \cdot 4H_2O$, ≥99% purity) and ferric chloride hexahydrate ($FeCl_3 \cdot 6H_2O$, ≥99% purity) were obtained from Merck KGaA (Darmstadt, Germany). Ammonia solution (25%) was purchased from Scharlau (Sentmenat, Barcelona, Spain). Deionized water was used in each experiment.

Synthesis of MNPs
The MNPs were prepared by a coprecipitation method as previously reported.[41] They were prepared by mixing solutions of 2.43 g of ferrous chloride tetrahydrate ($FeCl_2 \cdot 4H_2O$), 0.99 g ferric chloride hexahydrate ($FeCl_3 \cdot 6H_2O$), and 80 mL of deionized water in the presence of 6 mL of ammonia (25% by mass). The pH value of the solution was maintained at 10. Then the mixture was sonicated for 1 hour at room temperature. Finally, the precipitate was centrifuged and washed three times with deionized water.

Synthesis of CS-MNPs
The solution of CS was prepared by dissolving 1 g of CS powder in 1% acetic acid solution. It was followed by the addition of CS solution to MNPs suspension and then the mixture was stirred for 18 hours at room temperature. The obtained mixture was centrifuged and washed three times with deionized water and dried at 70°C. The product was labeled CS-MNPs.[23]

Synthesis of PTA-CS-MNP nanocomposite
The PTA-CS-MNP nanocomposite was obtained by mixing PTA sodium salt solution (2 g in 100 mL deionized water)

with a known amount of CS-MNPs. The solution was then kept under vigorous stirring for 24 hours. The final slurry was centrifuged, washed, and finally dried at 60°C oven.

Characterization of PTA-CS-MNP nanocomposite

The magnetic property of the samples was evaluated using Lake Shore 7404 vibrating sample magnetometer (Lake Shore Cryotronics, Inc., Westerville, OH, USA). The thermal analyses of the materials were performed using Mettler Toledo thermogravimetric (TGA) and differential thermogravimetric (DTG) instruments with a heating rate of 10°C per minute at temperature 20°C–1,000°C under nitrogen atmosphere (N_2 flow rate 50 mL per minute). Powder X-ray diffraction (PXRD) patterns were used to determine the crystal structures of the samples over a range of 5°–70°, using an XRD-6000 diffractometer (Shimadzu, Tokyo, Japan) with CuKα radiation (λ =1.5406 Å) at 30 kV and 30 mA. Fourier transform infrared (FTIR) spectra of the materials were recorded over a range of 400–4,000 cm^{-1}, using a Nexus, Smart Orbit spectrometer (Thermo Fisher Scientific, Waltham, MA, USA) and KBr disk method. The ultraviolet-visible (UV-Vis) spectrophotometer (Shimadzu 1650 series; Shimadzu) was used to determine the optical and controlled-release properties of PTA from PTA-CS-MNP nanocomposite. The mean particle size and size distribution were determined using a transmission electron microscope (Hitachi H-7100; Hitachi, Tokyo, Japan) at an accelerating voltage of 80 and 200 kV.

Loading and release of PTA from PTA-CS-MNP nanocomposite

The percentage of PTA loading in PTA-CS-MNP nanocomposite was measured using UV-Vis spectrophotometer (Shimadzu 1650 series; Shimadzu) and calibration curve equation. Approximately 5 mg of the nanocomposite was dissolved in concentrated HCl/HNO$_3$. In this condition 100% PTA content would be released from the nanocomposite. The amount of PTA released was measured by UV-Vis spectroscopy at a wavelength of 275 nm and using calibration curves.

PTA release profiles from the nanocomposite were determined at room temperature using 0.01 M phosphate-buffered saline (PBS) solution at pH 4.8 and 7.4. A total of 85 mg of PTA-CS-MNP nanocomposite was added to 500 mL of PBS medium. The cumulative amount of PTA released into the solution was measured at predetermined time intervals at λ$_{max}$ =275 nm using a UV-Vis spectrophotometer. The release rate of PTA from PTA-CS-MNP nanocomposite was compared with that from physical mixture that contained PTA sodium salt, CS, and MNPs.

Cytotoxicity assay of PTA-CS-MNP nanocomposite

HT-29 and 3T3 cells were obtained from American Type Culture Collection (ATCC, VA, USA), and these cells were cultured and plated at a density of 1×10^4 cells by adding 100 µL of cell suspension to each well of a 96-well tissue culture plate. The plates were incubated for sufficient time to ensure attachment of cells. The growth rate was ~70%–80% confluency. The media were aspirated off and replaced with fresh media (100 µL) containing different concentrations of PTA-CS-MNP nanocomposite as well as pure compound, PTA (25–500 µg/mL). The treated plates were incubated at 37°C in 5% CO$_2$ for 72 hours with appropriate control. After incubation with the compounds, 3-(4,5-dimethylthiazol-2-yl)-2,5-diphenyltetrazolium bromide (MTT) solution (5 mg/mL) in a total volume of 10 µL was added to every well and mixed gently with the media, which was later incubated for 4 hours at 37°C in 5% CO$_2$. The MTT solution containing the medium was then removed carefully and replaced with dimethyl sulfoxide (DMSO) (100 µL per well) to dissolve the formazan crystals. Finally, the culture plates were read in a microplate reader at 570 nm. The concentration of drug needed to inhibit cell growth by 50% (IC$_{50}$) was generated from the dose–response curves for each compound and each cell line.

Results and discussion
PXRD

Figure 1A–C illustrates the PXRD patterns of the MNPs, PTA-CS-MNP, and PTA sodium salt, respectively. For MNPs and PTA-CS-MNP nanocomposite, six characteristic peaks at 2θ=30.2°, 35.5°, 43.2°, 53.5°, 57.2°, and 62.7° were indexed to (220), (311), (400), (422), (511), and (440), respectively, (JCPDS No 19-629) which are due to the cubic spinel structure of pure Fe$_3$O$_4$.[42] Figure 1A and B reveals that the coating process did not affect the phase change of MNPs as there is no changes in the position of the peaks.[43] However, the coating process resulted in a lower peak intensity and crystallinity of the PTA-CS-MNP nanocomposite. The mean grain size was calculated from XRD data by Debye-Scherrer equation that determines the connection between average particle size and peak broadening in XRD.

$$D = \frac{K\lambda}{\beta\cos\theta}$$

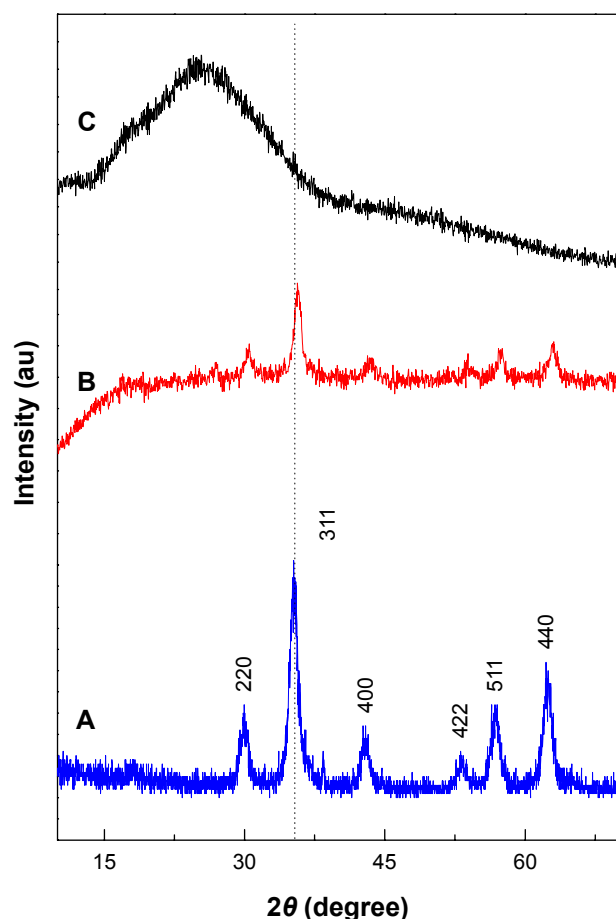where D is the average particle size, K is the Debye-Scherrer constant (0.89), λ is the X-ray wavelength (0.15406 nm),

Figure 1 Powder X-ray diffraction patterns of iron oxide magnetic nanoparticles (**A**), PTA-CS-MNP nanocomposite (**B**), and phytic acid sodium salt (**C**).
Abbreviation: PTA-CS-MNP, phytic acid-chitosan-iron oxide nanocomposite.

Figure 2 Fourier transform infrared spectra of iron oxide magnetic nanoparticles (**A**), PTA-CS-MNP nanocomposite (**B**), and phytic acid sodium salt (**C**).
Abbreviation: PTA-CS-MNP, phytic acid-chitosan-iron oxide nanocomposite.

β is the peak width of half-maximum, and θ is the diffraction angle. The mean particle size of MNPs obtained from this equation was ~8 nm.

FTIR spectroscopy

The FTIR spectra of MNPs, PTA-CS-MNP nanocomposite, and PTA sodium salt are presented in Figure 2. The MNPs in Figure 2A shows an absorption peak at 569 cm^{-1} that is due to the stretching of Fe-O in Fe_3O_4. However, this peak was shifted to 565 cm^{-1} in the PTA-CS-MNP nanocomposite (Figure 2B), which confirm the presence of MNPs in the nanocomposites.[44] The broad absorption peak observed at 3,415 cm^{-1} in Figure 2A is ascribed to the O–H stretching. In the PTA-CS-MNP nanocomposite spectra (Figure 2B), the characteristic band for CS was observed at 1,560 cm^{-1}, which proves that MNPs were successfully coated with CS.[45]

The FTIR spectra of PTA sodium salt shown in Figure 2C displays some intense, sharp absorption peaks due
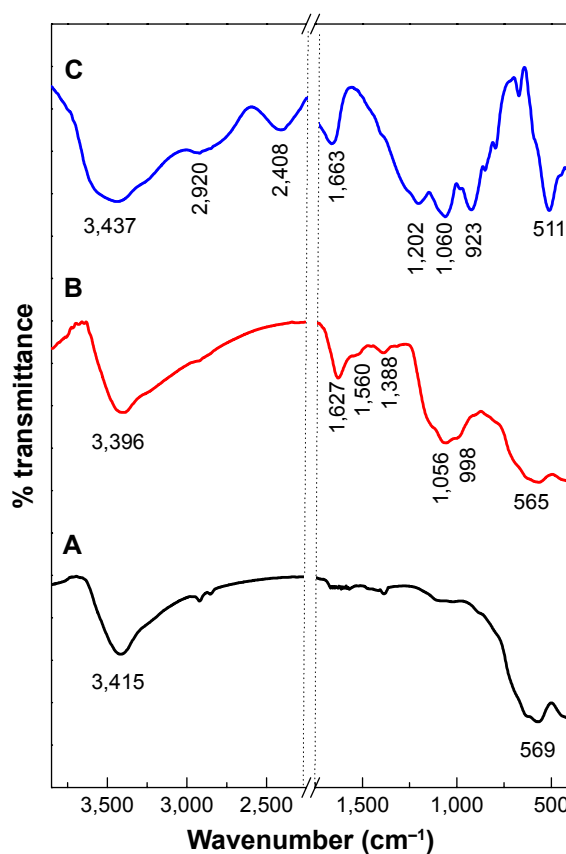
to different functional groups in the molecules. The characteristic bands at 1,202 and 1,060 cm^{-1} can be assigned to the stretching vibration of P=O and P–O–C, respectively, and in the nanocomposite spectrum (Figure 2B), the bands shifted to 1,388 and 1,056 cm^{-1}, respectively, due to coating process. The stretch at 511 cm^{-1} corresponded to the O–Na and O–P=O vibrations were revealed at 2,408 and 2,920 cm^{-1} (Figure 2C).[46] The absorption peaks of OH group of water molecules present in the PTA sodium salt appeared at 1,663 and 3,437 cm^{-1},[46] while the peaks were recorded at 1,627 and 3,396 cm^{-1} in the nanocomposite spectra (Figure 2B).

Figure 3 shows the interaction between the MNPs, CS, and PTA. It is clear that MNPs interacted with CS through glycosidic bonds (Figure 3A), whereas PTA (Figure 3B) interacted with CS polymer through hydrogen bonds.[47,48]

Thermal analysis

The thermal behavior of PTA sodium salt, MNPs, and PTA-CS-MNP nanocomposite was examined by TGA and DTG
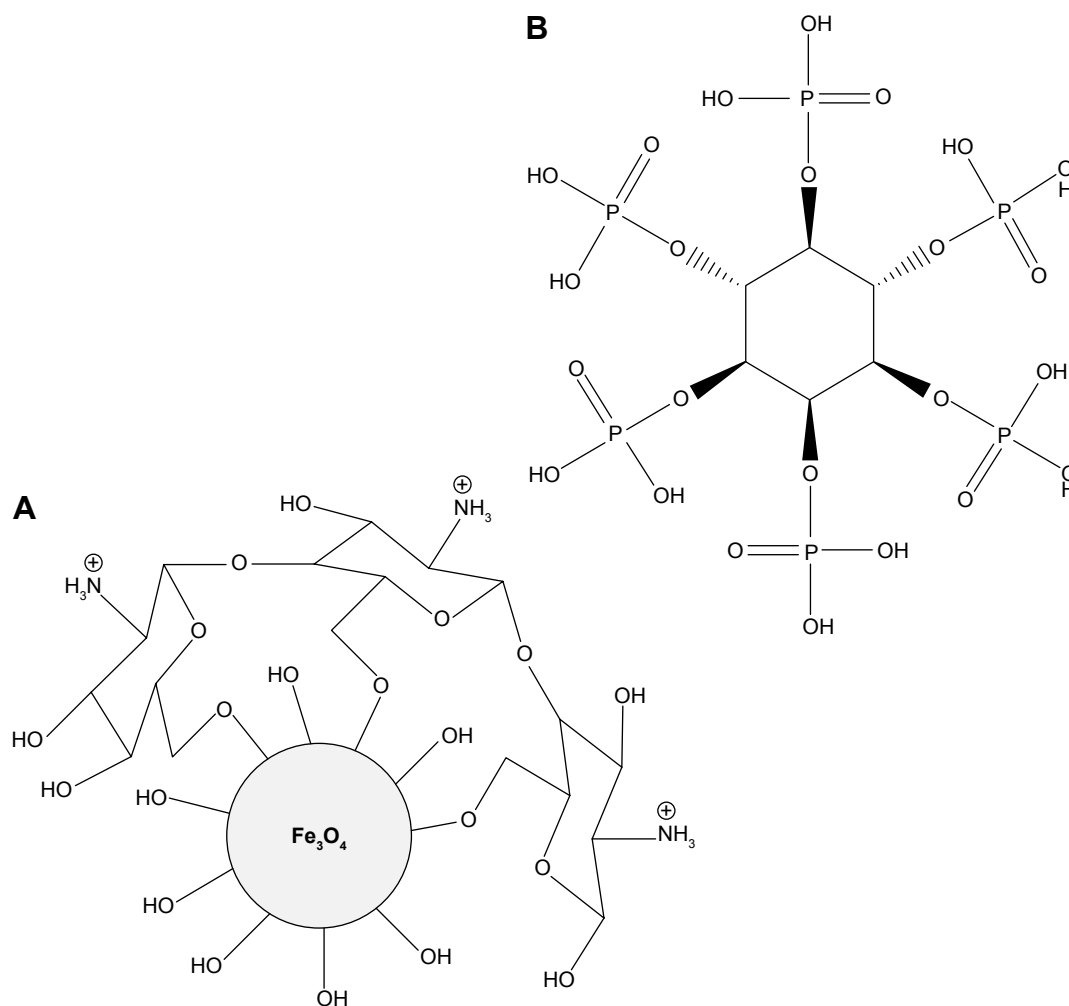
Figure 3 Schematic representation of the interaction between iron oxide magnetic nanoparticles, chitosan (**A**), and phytic acid (**B**) in the PTA-CS-MNP nanocomposite.
Abbreviation: PTA-CS-MNP, phytic acid-chitosan-iron oxide nanocomposite.

analyses (Figure 4). The PTA sodium salt thermal decomposition (Figure 4A) showed three weight loss events. The first event occurred at 123°C with a weight loss of 25.9%, which was due to the removal of water present in the sample. The second weight loss of 20.6% at 205°C might be due to the carbonization process and dehydration that takes place due to the decomposition of OH groups. This third one was followed by the decomposition of phytate groups and the elimination of elemental carbon formed in the previous step at 309°C with a mass reduction of 41.2%.[49] The TGA/DTG thermograms of MNPs (Figure 4B) exhibited a single-stage mass reduction at 44°C with a weight loss of 9.7%, which can be attributed to the loss of surface hydroxyl groups and residual water.[25] For PTA-CS-MNP nanocomposite, three main thermal phenomena were observed (Figure 4C). The first weight loss of 9.6% at 62°C was related to the removal of surface physisorbed water molecules. The second and third weight loses of 23.4% and 12.1% at 242°C and 610°C,

respectively, corresponded to the decomposition of PTA and CS biopolymer. The temperature region of the nanocomposite appeared to be clearly higher than that of the free drug due to the electrostatic attraction between the MNPs, CS, and PTA.

Magnetic properties

Superparamagnetism is an essential and important property for magnetic-targeting carriers in drug-delivery system.[50] Magnetic properties of MNPs and PTA-CS-MNP nanocomposite were characterized by vibrating sample magnetometer as a function of the magnetic field at room temperature (Figure 5). The saturation magnetization of MNPs was 53.25 emu/g compared to that of PTA-CS-MNP nanocomposite which was 42.15 emu/g, and negligible coercivity and remanent magnetization were observed for both samples, which confirmed the superparamagnetic properties of the samples. The decrease in saturation magnetization of
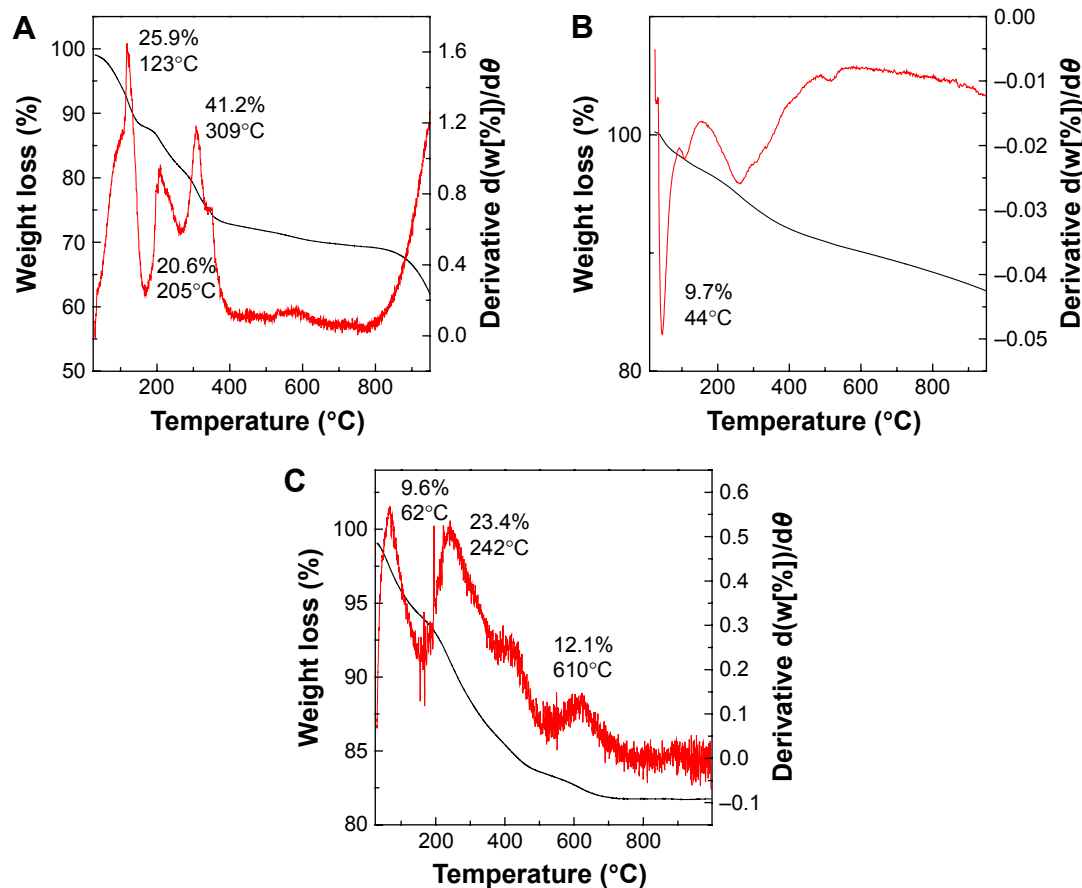
Figure 4 TGA/DTG thermograms of phytic acid sodium salt (**A**), iron oxide magnetic nanoparticles (**B**), and PTA-CS-MNP nanocomposite (**C**).
Abbreviations: PTA-CS-MNP, phytic acid-chitosan-iron oxide nanocomposite; TGA/DTG, thermogravimetric and differential thermogravimetric analyses.

PTA-CS-MNPs nanocomposite could be due to the existence of coated materials on the surface of MNPs and electron exchange between CS polymer coating and Fe atoms.[51–53] This could affect surface magnetic anisotropy and enhance surface spins disorientation.[54]
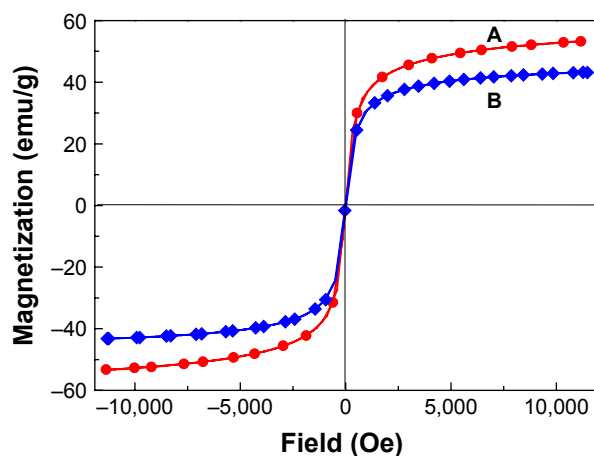

Figure 5 Magnetization curves of iron oxide magnetic nanoparticles (**A**) and phytic acid-loaded chitosan-iron oxide magnetic nanoparticles (**B**) recorded at room temperature.
Abbreviation: Oe, oersted.

Determination of average size and size distribution properties

Transmission electron microscopy images and size distribution of pristine Fe_3O_4, CS-MNPs, and PTA-CS-MNP nanocomposite are presented in Figure 6. The images show that nanosized particles were successfully prepared using coprecipitation method, and all the samples such as MNPs, CS-MNPs, and PTA-CS-MNP nanocomposite showed roughly spherical shape (Figure 6A–C). The average size of MNPs was ~15±6 nm (Figure 6D), whereas the mean sizes of CS-MNPs and PTA-CS-MNP nanocomposite were around 12±4 nm and 8±3 nm, respectively (Figure 6E and F). The decrease in the size of CS-MNPs and PTA-CS-MNP nanocomposite after coating might be due to prolonged vigorous stirring at high speeds after adding CS and PTA.[52]

In vitro release study of PTA from PTA-CS-MNP nanocomposite

The UV-Vis absorption spectroscopy and calculations by calibration curve equation showed that the percentage
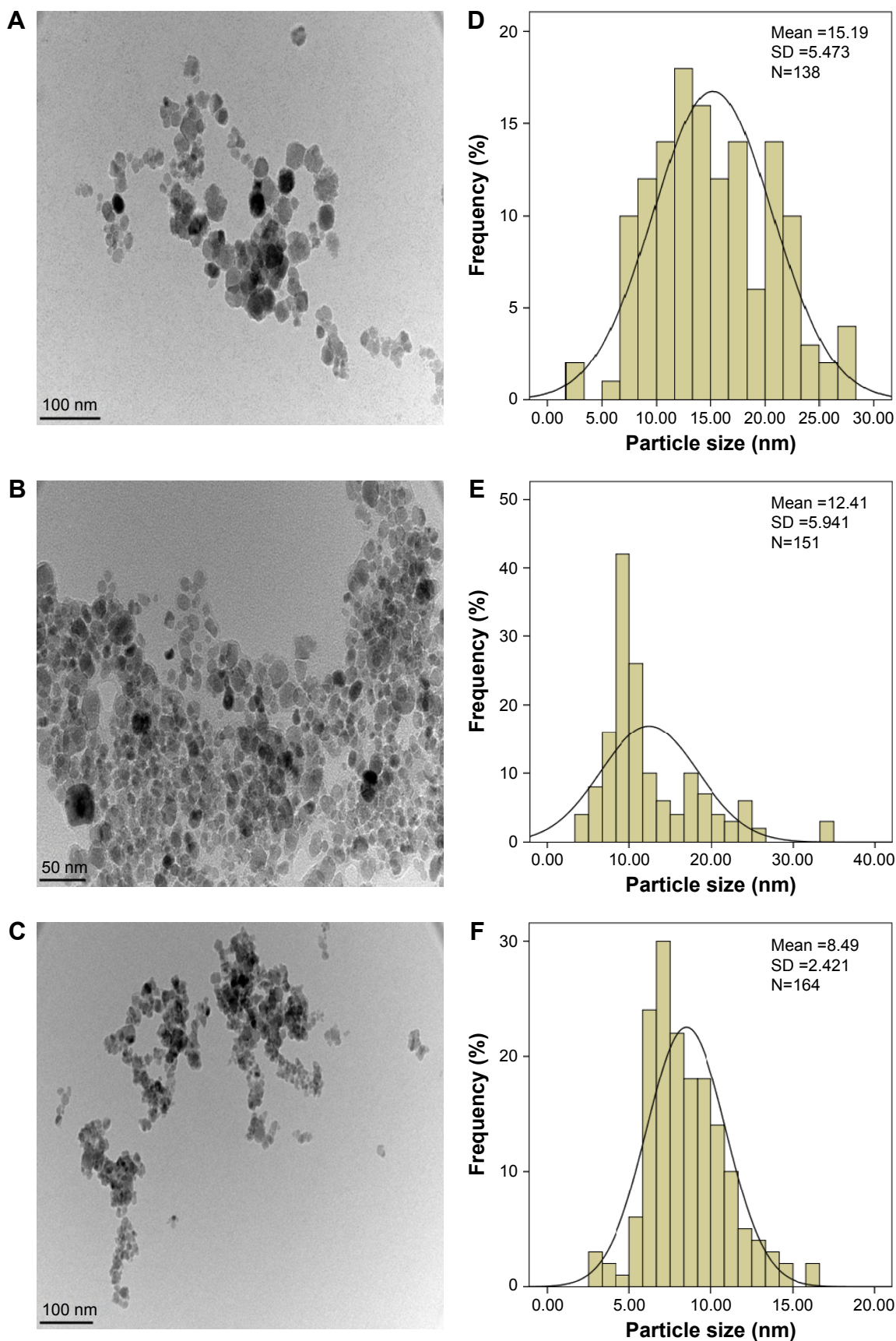
Figure 6 TEM micrographs of iron oxide magnetic nanoparticles (**A**), chitosan-iron oxide magnetic nanoparticles (**B**), and PTA-CS-MNP nanocomposite (**C**). Particle size distribution of iron oxide magnetic nanoparticles (**D**), chitosan-iron oxide magnetic nanoparticles (**E**), and PTA-CS-MNP nanocomposite (**F**).
Abbreviations: PTA-CS-MNP, phytic acid-chitosan-iron oxide nanocomposite; TEM, transmission electron microscopy.

loading of PTA in the PTA-CS-MNP nanocomposite was 12.9%. The release profiles of PTA from the PTA-CS-MNP nanocomposite and physical mixture are shown in Figure 7. The physical mixture of PTA sodium salt with CS and MNPs exposed to pH 4.8 or pH 7.4 environment shows that the release of PTA was fast and completed within 60 seconds (inset in Figure 7). However, the release rate of PTA from the PTA-CS-MNP nanocomposite was markedly slower than that from the physical mixture, indicating that the PTA-CS-MNP nanocomposite is a potential controlled release drug-delivery system. This result may be attributed to the interaction between the negatively charged PTA and positively charged protonated CS.

The release rate of PTA from PTA-CS-MNP nanocomposite is dependent on the pH of the environment; the release rate of PTA at pH 7.4 was remarkably lower than that at pH 4.8. Figure 7 shows that the percent release of drug from nanocomposite reached 93% within 56 hours when exposed to a pH environment of 4.8 and 86% by 127 hours at pH 7.4 PBS.

Such a difference in the release rate at pH 4.8 and 7.4 might be due to a possible difference in the release mechanism of PTA from the nanocomposite. At acidic pH (pH 4.8), PTA-CS-MNP nanocomposite is unstable, but at pH 7.4, it is more stable.[55,56] As a result, the release would occur through ion exchange between PTA anions and negative anions available on the PBS.

Release kinetics of PTA from PTA-CS-MNP nanocomposite

A number of kinetic models describe the total release of PTA from PTA-CS-MNP nanocomposite. The common models used include pseudo-first order, pseudo-second order, and parabolic diffusion models. Pseudo-first order kinetic equation is written as follows:[57]

$$\ln(q_e - q_t) = \ln q_e - kt$$

where q_e and q_t are the equilibrium release amount and the release amount at time t, respectively, and k is the constant of the corresponding release rate.

In pseudo-second order kinetic model, the release behavior of drugs from nanocomposite is described by the following equation:[58]

$$t/q_t = 1/kq_e^2 + t/q_e$$

By plotting t/q_t against t, a straight line is obtained and the release rate constant k, as well as q_e, can be calculated using a the following relation:

$$k = 1/q_e^2 . \text{intercept}$$

The parabolic diffusion kinetic model is written as follows:[59]

$$\frac{(1 - M_t/M_o)}{t} = kt^{-0.5} + b$$

where M_o and M_t are the PTA content that remain in the nanocomposite at release time 0 and t, respectively.

Among these three kinetic models, it was found that the release kinetic processes of PTA from PTA-CS-MNP nanocomposite at pH 7.4 and 4.8 were well governed by the pseudo-second order model, with correlation coefficients of (R^2) 0.9996 and 0.9980 and release rate constant (k) values of 1.69×10^{-5} and 2.86×10^{-5} mg/min, respectively (Figure 8 and Table 1).

The results of kinetic model gained in this work are similar to the release kinetic study of the chlorogenic acid intercalated into the Zn/Al-LDH, Mg/Al-LDH by ion-exchange and coprecipitation routes and ZLH[58,60,61] and also very similar to release of protocatechuic acid from Zn/Al-layered double hydroxide and zinc layered hydroxide.[62,63]
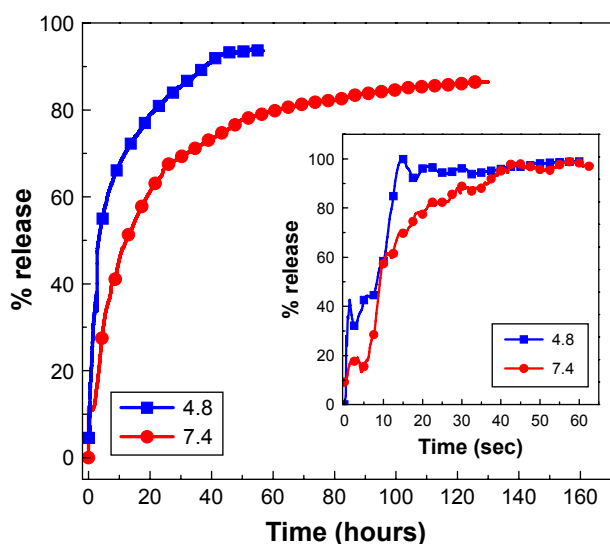

Figure 7 Release profiles of phytic acid from PTA-CS-MNP nanocomposite into phosphate-buffered saline solution at pH 7.4 and pH 4.8. The inset shows the release profiles of a physical mixture of phytic acid sodium salt with chitosan and iron oxide nanoparticles into phosphate-buffered saline solution at pH 7.4 and pH 4.8.
Abbreviation: PTA-CS-MNP, phytic acid-chitosan-iron oxide nanocomposite.
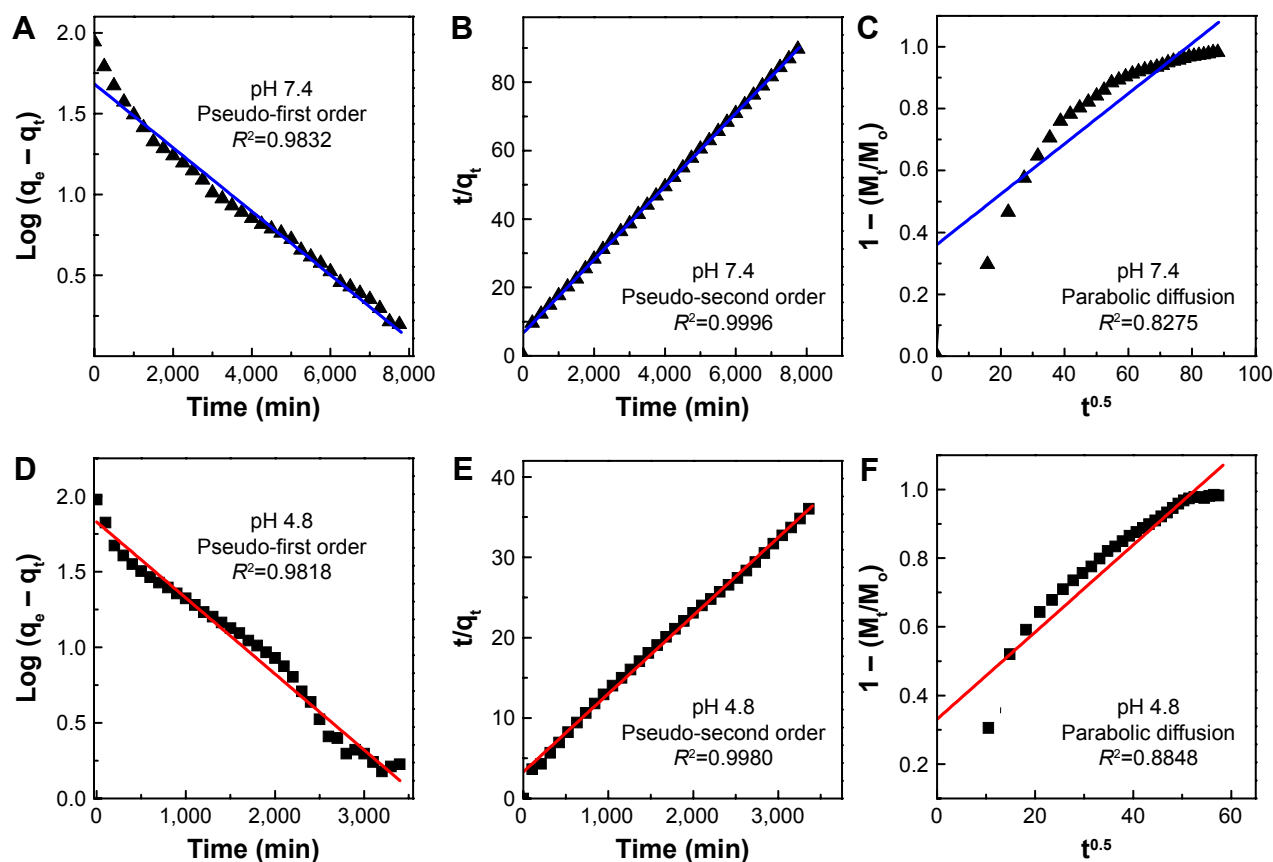
Figure 8 Fitting of the data for phytic acid release from PTA-CS-MNP nanocomposite into various solutions to the pseudo-first order, pseudo-second order kinetics and parabolic diffusion model for pH 7.4 (**A–C**) and pH 4.8 (**D–F**).
Abbreviation: PTA-CS-MNP, phytic acid-chitosan-iron oxide nanocomposite.

Cellular sensitivity of cells to PTA and PTA-CS-MNP nanocomposite

The efficacy of PTA-CS-MNP nanocomposite in suppressing the growth of HT29 colorectal adenocarcinoma cells was assessed using colorimetric assay (MTT assay). The 3T3 normal fibroblast cells were employed as normal control to ensure the nontoxic nature of nanocomposite. As illustrated in Figure 9B, HT29 cells displayed a dose-dependent reduction in cell viability after 72 hours of incubation with nanocomposite. PTA-CS-MNP nanocomposite exerted a cytotoxic effect on HT29 at higher concentrations and showed a moderate inhibition at lower concentrations. In general, pure compound exhibited a much lower cytotoxic effect on HT29 cells with a higher half maximal inhibitory concentration value (IC_{50}) of 188.5 µg/mL compared to PTA-CS-MNP nanocomposite, whose IC_{50} value was 45.63 µg/mL. This shows that the introduction of CS-MNPs into PTA improved the efficacy of PTA in HT29 cells. It is apparent from Figure 9A that both free PTA and nanocomposite did not induce toxicity in 3T3 normal fibroblast cells. Both compounds did not affect cell viability in the tested range, as the survival was consistently greater than 80% or similar

Table 1 Correlation coefficient (R^2), rate constant (k), and half-life ($t_{1/2}$) values obtained by fitting the release data of phytic acid from PTA-CS-MNP nanocomposite into phosphate-buffered saline solution at pH 4.8 and 7.4

Aqueous solution	Saturation release (%)	R^2			Pseudo-second order model	
		Pseudo-first order model	Pseudo-second order model	Parabolic diffusion	Rate constant, k (mg/min)	$t_{1/2}$ (min)
pH 7.4	86	0.9832	0.9996	0.8275	1.69×10^{-5}	630
pH 4.8	93	0.9818	0.9980	0.8848	2.86×10^{-5}	339

Abbreviation: PTA-CS-MNP, phytic acid-chitosan-iron oxide nanocomposite.
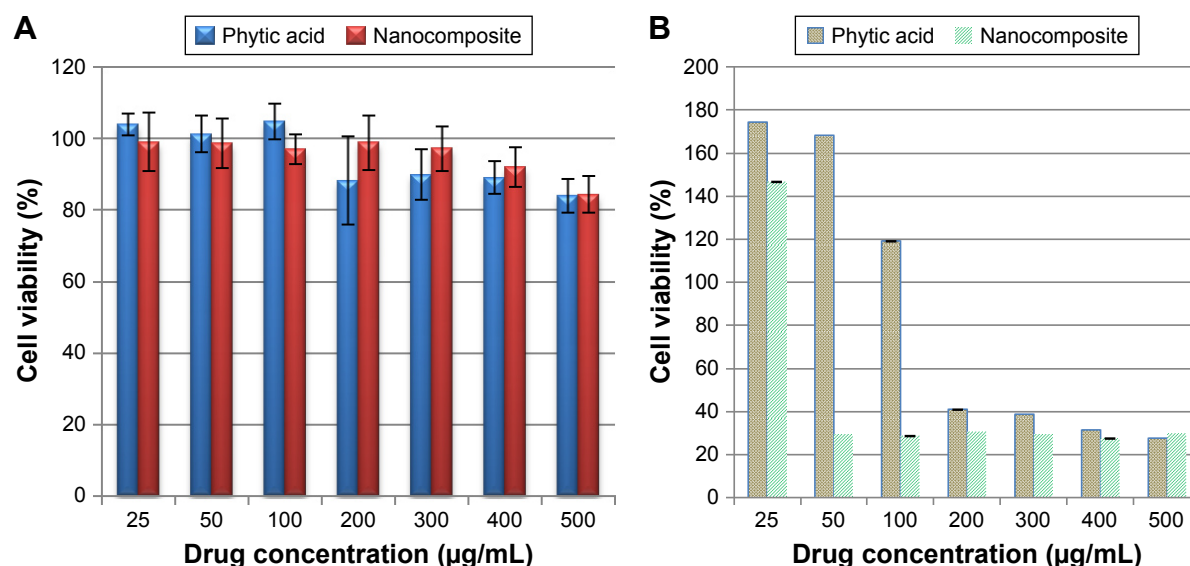
Figure 9 Cell viability (MTT assay) of 3T3 (**A**) and HT29 (**B**) cells exposed to various gradient concentrations. The data are presented as mean ± standard deviation of triplicate values.
Abbreviation: MTT, 3-(4,5-dimethylthiazol-2-yl)-2,5-diphenyltetrazolium bromide.

to control. In this case, it can be suggested that PTA-CS-MNP nanocomposite possessed good anticancer activities when compared with pure compound PTA and demonstrated selectivity between cancerous and normal cells.

Conclusion

PTA-CS-MNP nanocomposite was successfully prepared by coating MNPs with CS and then loading it with PTA drug. The loading percentage of PTA into the nanocomposite was 12.9% and the superparamagnetic properties of PTA-CS-MNP nanocomposite and MNPs were shown by vibrating sample magnetometry studies. The vibration modes of the coated CS to MNPs and loaded PTA, which supported the formation of PTA-CS-MNP nanocomposite, were confirmed by FTIR. The release profiles of the drug from nanocomposite into PBS were of sustained manner with total release equilibria of 86% and 93% when exposed to environments of pH 7.4 and 4.8 at 127 and 56 hours, respectively. The pseudo-second order kinetics model was found to be the best fitting mathematical model. Overall, the findings of this study suggest that PTA-CS-MNP nanocomposites possess good anticancer potential against colon cancer cells and do not cause any cytotoxicity to normal fibroblast cells. Further, cellular and molecular studies are needed to find out the specific cellular mechanism that describes the specific action of nanocomposite against colon cancer cells. Also, in vivo studies are to be carried out to prove the therapeutic potential of the present tumor-specific delivery system.

Disclosure

The authors report no conflicts of interest in this work.

References

1. Boisseau P, Loubaton B. Nanomedicine, nanotechnology in medicine. *Comptes Rendus Physique*. 2011;12(7):620–636.
2. Misra R, Acharya S, Sahoo SK. Cancer nanotechnology: application of nanotechnology in cancer therapy. *Drug Discov Today*. 2010;15(19–20): 842–850.
3. Nguyen TX, Huang L, Gauthier M, Yang G, Wang Q. Recent advances in liposome surface modification for oral drug delivery. *Nanomedicine (Lond)*. 2016;11(9):1169–1185.
4. Li MH, Yu H, Wang TF, et al. Tamoxifen embedded in lipid bilayer improves the oncotarget of liposomal daunorubicin in vivo. *J Mater Chem B*. 2014;2(12):1619–1625.
5. Du D, Chang N, Sun S, et al. The role of glucose transporters in the distribution of p-aminophenyl-α-d-mannopyranoside modified liposomes within mice brain. *J Control Release*. 2014;182:99–110.
6. Cao J, Wang R, Gao N, et al. A7RC peptide modified paclitaxel liposomes dually target breast cancer. *Biomater Sci*. 2015;3(12): 1545–1554.
7. Wang Q, Cheng H, Peng H, Zhou H, Li PY, Langer R. Non-genetic engineering of cells for drug delivery and cell-based therapy. *Adv Drug Deliv Rev*. 2015;91:125–140.
8. Peng H, Liu X, Wang G, et al. Polymeric multifunctional nanomaterials for theranostics. *J Mater Chem B*. 2015;3(34):6856–6870.
9. McCallion C, Burthem J, Rees-Unwin K, Golovanov A, Pluen A. Graphene in therapeutics delivery: problems, solutions and future opportunities. *Eur J Pharm Biopharm*. 2016;104:235–250.
10. Barahuie F, Saifullah B, Dorniani D, et al. Graphene oxide as a nanocarrier for controlled release and targeted delivery of an anticancer active agent, chlorogenic acid. *Mater Sci Eng C*. 2017;74:177–185.

11. Kesharwani P, Jain K, Jain NK. Dendrimer as nanocarrier for drug delivery. *Prog Polym Sci*. 2014;39:268–307.

12. Peng H, Wang C, Xu X, Yu C, Wang Q. An intestinal Trojan horse for gene delivery. *Nanoscale*. 2015;7(10):4354–4360.

13. Barahuie F, Hussein MZ, Fakurazi S, Zainal Z. Development of drug delivery systems based on layered hydroxides for nanomedicine. *Int J Mol Sci*. 2014;15(5):7750–7786.

14. Parsian M, Unsoy G, Mutlu P, Yalcin S, Tezcaner A, Gunduz U. Loading of Gemcitabine on chitosan magnetic nanoparticles increases the anti-cancer efficacy of the drug. *Eur J Pharmacol*. 2016;784:121–128.

15. Xiao Y, Lin ZT, Chen Y, et al. High molecular weight chitosan derivative polymeric micelles encapsulating superparamagnetic iron oxide for tumor-targeted magnetic resonance imaging. *Int J Nanomedicine*. 2015;10:1155–1172.

16. Zhao YB, Qiu ZM, Huang JY. Preparation and analysis of Fe₃O₄ magnetic nanoparticles used as targeted-drug carriers. *Chinese J Chem Eng*. 2008;16(3):451–455.

17. Ghotbi MY, bin Hussein MZ. Controlled release study of an anti-carcinogenic agent, gallate from the surface of magnetite nanoparticles. *J Phys Chem Solids*. 2012;73(7):936–942.

18. Ahmad T, Rhee I, Hong S, Chang Y, Lee J. Ni-Fe₂O₄ nanoparticles as contrast agents for magnetic resonance imaging. *J Nanosci Nanotechnol*. 2011;11(7):5645–5650.

19. Laurent S, Forge D, Port M, et al. Magnetic iron oxide nanoparticles: synthesis, stabilization, vectorization, physicochemical characterizations, and biological applications. *Chem Rev*. 2008;108(6):2064–2110.

20. Parveen S, Misra R, Sahoo SK. Nanoparticles: a boon to drug delivery, therapeutics, diagnostics and imaging. *Nanomedicine*. 2012;8(2):147–166.

21. Béalle G, Di Corato R, Kolosnjaj-Tabi J, et al. Ultra magnetic liposomes for MR imaging, targeting, and hyperthermia. *Langmuir*. 2012;28(32):11834–11842.

22. Hirsch LR, Stafford RJ, Bankson JA, et al. Nanoshell-mediated near-infrared thermal therapy of tumours under magnetic resonance guidance. *Proc Natl Acad Sci U S A*. 2003;100(23):13549–13554.

23. Qu J, Liu G, Wang Y, Hong R. Preparation of Fe₃O₄-chitosan nanoparticles used for hyperthermia. *Adv Powder Technol*. 2010;21(4):461–467.

24. Denkbaş EB, Kiliçay E, Birlikseven C, Öztürk E. Magnetic chitosan microspheres: preparation and characterization. *React Funct Polym*. 2002;50(3):225–232.

25. Li GY, Jiang YR, Huang KL, Ding P, Chen J. Preparation and properties of magnetic Fe₃O₄–chitosan nanoparticles. *J Alloys Compd*. 2008;466(1):451–456.

26. Artursson P, Lindmark T, Davis SS, Illum L. Effect of chitosan on the permeability of monolayers of intestinal epithelial cells (Caco-2). *Pharm Res*. 2004;11(9):1358–1361.

27. Hejazi R, Amiji M. Chitosan-based gastrointestinal delivery systems. *J Control Release*. 2003;89(2):151–165.

28. Miao Y, Tan SN. Amperometric hydrogen peroxide biosensor based on immobilization of peroxidase in chitosan matrix crosslinked with glutaraldehyde. *Analyst*. 2000;125(9):1591–1594.

29. Ravi Kumar MN. A review of chitin and chitosan applications. *React Funct Polym*. 2000;46(1):1–27.

30. Rabea EI, Badawy ME, Stevens CV, Smagghe G, Steurbaut W. Chitosan as antimicrobial agent: applications and mode of action. *Biomacromolecules*. 2003;4(6):1457–1465.

31. Hussein-Al-Ali SH, El Zowalaty ME, Hussein MZ, Geilich BM, Webster TJ. Synthesis, characterization, and antimicrobial activity of an ampicillin-conjugated magnetic nanoantibiotic for medical applications. *Int J Nanomedicine*. 2014;9:3801–3814.

32. Javid A, Ahmadian S, Saboury AA, Kalantar SM, Rezaei-Zarch S. Chitosan-coated superparamagnetic iron oxide nanoparticles for doxorubicin delivery: synthesis and anticancer effect against human ovarian cancer cells. *Chem Biol Drug Des*. 2013;82(3):296–306.

33. Canan C, Cruz FT, Delaroza F, et al. Studies on the extraction and purification of phytic acid from rice bran. *J Food Comp Anal*. 2011;24(7):1057–1063.

34. Irshad M, Ahmad I, Mehdi SJ, Goel HC, Rizvi MM. Antioxidant capacity and phenolic content of the aqueous extract of commonly consumed cucurbits. *Int J Food Prop*. 2014;17(1):179–186.

35. Canan C, Delaroza F, Casagrande R, Baracat MM, Shimokomaki M, Ida EI. Antioxidant capacity of phytic acid purified from rice bran. *Acta Sci Technol*. 2012;34(4):457–463.

36. Tan BL, Norhaizan ME. Scientific evidence of rice by-products for cancer prevention: chemopreventive properties of waste products from rice milling on carcinogenesis in vitro and in vivo. *Bio Med Res Int*. 2017;2017:9017902.

37. Henderson AJ, Ollila CA, Kumar A, et al. Chemopreventive properties of dietary rice bran: current status and future prospects. *Adv Nutr*. 2012;3:643–653.

38. Norhaizan ME, Ng SK, Norashareena MS, Abdah MA. Antioxidant and cytotoxicity effect of rice bran phytic acid as an anticancer agent on ovarian, breast and liver cancer cell lines. *Malays J Nutr*. 2011;17(3):367–375.

39. Norazalina S, Norhaizan ME, Hairuszah I, Norashareena MS. Anticarcinogenic efficacy of phytic acid extracted from rice bran on azoxymethane-induced colon carcinogenesis in rats. *Exp Toxicol Pathol*. 2010;62(3):259–268.

40. Al-Fatlawi AA, Rizvi MM, Ahmad A. Anticarcinogenic activity of rice bran phytic acid against human breast cancer cell line (mcf-7). *Asian J Pharm Clin Res*. 2014;7(1):151–155.

41. Lee H, Shao H, Huang Y, Kwak B. Synthesis of MRI contrast agent by coating superparamagnetic iron oxide with chitosan. *IEEE Trans Magn*. 2005;41(10):4102–4104.

42. Calmon MF, de Souza AT, Candido NM, et al. A systematic study of transfection efficiency and cytotoxicity in HeLa cells using iron oxide nanoparticles prepared with organic and inorganic bases. *Colloids Surf B Biointerfaces*. 2012;100:177–184.

43. Dodi G, Hritcu D, Lisa G, Popa MI. Core–shell magnetic chitosan particles functionalized by grafting: synthesis and characterization. *Chem Eng J*. 2012;203:130–141.

44. Unsoy G, Yalcin S, Khodadust R, Gunduz G, Gunduz U. Synthesis optimization and characterization of chitosan-coated iron oxide nanoparticles produced for biomedical applications. *J Nanopart Res*. 2012;14(11):964.

45. Marchessault RH, Ravenelle F, Zhu XX, editors. *Polysaccharides for Drug Delivery and Pharmaceutical Applications*. Vol 934. Washington, DC: American Chemical Society; 2006.

46. Saburov KA, Kamilov KM. Structure of phytic acid and phytates. *Chem Nat Compd*. 1989;25(6):695–698.

47. Qu JB, Shao HH, Jing GL, Huang F. PEG-chitosan-coated iron oxide nanoparticles with high saturated magnetization as carriers of 10-hydroxycamptothecin: preparation, characterization and cytotoxicity studies. *Colloids Surf B Biointerfaces*. 2013;102:37–44.

48. Hussein-Al-Ali SH, El Zowalaty ME, Hussein MZ, Ismail M, Webster TJ. Synthesis, characterization, controlled release, and antibacterial studies of a novel streptomycin chitosan magnetic nanoantibiotic. *Int J Nanomedicine*. 2014;9:549–557.

49. Daneluti AL, Velasco MV, Baby AR, Matos JD. Thermal behavior and free-radical-scavenging activity of phytic acid alone and incorporated in cosmetic emulsions. *Cosmetics*. 2015;2(3):248–258.

50. Kayal S, Ramanujan RV. Doxorubicin loaded PVA coated iron oxide nanoparticles for targeted drug delivery. *Mater Sci Eng C*. 2010;30(3):484–490.

51. Kumar R, Inbaraj BS, Chen BH. Surface modification of superparamagnetic iron nanoparticles with calcium salt of poly (γ-glutamic acid) as coating material. *Mater Res Bull*. 2010;45(11):1603–1607.

52. Yu S, Chow GM. Carboxyl group (-CO₂H) functionalized ferrimagnetic iron oxide nanoparticles for potential bio-applications. *J Mater Chem*. 2004;14(18):2781–2786.

53. Shan Z, Yang WS, Zhang X, Huang QM, Ye H. Preparation and characterization of carboxyl-group functionalized superparamagnetic nanoparticles and the potential for bio-applications. *J Braz Chem Soc*. 2007;18(7):1329–1335.

54. Ge Y, Zhang Y, Xia J, et al. Effect of surface charge and agglomerate degree of magnetic iron oxide nanoparticles on KB cellular uptake in vitro. *Colloids Surf B Biointerfaces*. 2009;73(2):294–301.

55. Barahuie F, Hussein MZ, Hussein-Al-Ali SH, Arulselvan P, Fakurazi S, Zainal Z. Preparation and controlled-release studies of protocatechuic acid-magnesium/aluminium-layered double hydroxide nanocomposite. *Int J Nanomedicine*. 2013;8:1975–1987.

56. Khan AI, O'Hare D. Intercalation chemistry of layered double hydroxides: recent developments and applications. *J Mater Chem*. 2002; 12(11):3191–3198.

57. Dong L, Yan L, Hou WG, Liu SJ. Synthesis and release behavior of composites of camptothecin and layered double hydroxide. *J Solid State Chem*. 2010;183(8):1811–1816.

58. Barahuie F, Hussein MZ, Arulselvan P, Fakurazi S, Zainal Z. Development of the anticancer potential of a chlorogenate-zinc layered hydroxide nanohybrid with controlled release property against various cancer cells. *Sci Adv Mater*. 2013;5(12):1983–1993.

59. Ho YS, Ofomaja AE. Pseudo-second-order model for lead ion sorption from aqueous solutions onto palm kernel fiber. *J Hazard Mater*. 2006; 129(1–3):137–142.

60. Barahuie F, Hussein MZ, Arulselvan P, Fakurazi S, Zainal Z. Drug delivery system for an anticancer agent, chlorogenate-Zn/Al-layered double hydroxide nanohybrid synthesised using direct co-precipitation and ion exchange methods. *J Solid State Chem*. 2014;217:31–41.

61. Barahuie F, Hussein MZ, Arulselvan P, Fakurazi S, Zainal Z. Controlled in vitro release of the anticancer drug chlorogenic acid using magnesium/aluminium-layered double hydroxide as a nanomatrix. *Sci Adv Mater*. 2016;8(3):501–513.

62. Barahuie F, Hussein MZ, Abd Gani S, Fakurazi S, Zainal Z. Synthesis of protocatechuic acid-zinc/aluminium layered double hydroxide nanocomposite as an anticancer nanodelivery system. *J Solid State Chem*. 2015;221:21–31.

63. Barahuie F, Hussein MZ, Abd Gani S, Fakurazi S, Zainal Z. Anticancer nanodelivery system with controlled release property based on protocatechuate-zinc layered hydroxide nanohybrid. *Int J Nanomedicine*. 2014;9:3137–3149.